European Journal of Pharmaceutics and Biopharmaceutics 124 (2018) 63–72

Contents lists available at ScienceDirect

European Journal of Pharmaceutics and Biopharmaceutics

journal homepage: www.elsevier.com/locate/ejpb

Research paper

The effect of subcellular localization on the efficiency of EGFR-targeted VHH photosensitizer conjugates

Sanne A.M. van Lith[a], Dirk van den Brand[b,c], Rike Wallbrecher[b], Lina Wübbeke[a], Sander M.J. van Duijnhoven[a], Petri I. Mäkinen[d], Janneke S. Hoogstad-van Evert[c], Leon Massuger[c], Seppo Ylä-Herttuala[d,e], Roland Brock[b], William P.J. Leenders[a,b,*]

[a] Department of Pathology, Radboudumc, Geert Grooteplein zuid 10, 6525 GA Nijmegen, The Netherlands
[b] Department of Biochemistry, Radboudumc, Geert Grooteplein 28, 6525 GA Nijmegen, The Netherlands
[c] Department of Obstetrics and Gynaecology, Radboudumc, Geert Grooteplein zuid 10, 6525 GA Nijmegen, The Netherlands
[d] A.I. Virtanen Institute for Molecular Sciences, University of Eastern Finland, P.O. Box 1627, Kuopio, Finland
[e] Heart Center, Kuopio University Hospital, 70211 Kuopio, Finland

ARTICLE INFO

Keywords:
Photodynamic therapy
Nanobody/VHH
Cell-penetrating peptide
Ovarian cancer
EGFR
Site specific conjugation

ABSTRACT

Photodynamic therapy (PDT) is an emerging method to treat light-accessible malignancies. To increase specificity and allow dose reduction, conjugates of photosensitizers (PS) with antibodies against tumor-associated antigens have been developed for photoimmunotherapy (PIT). However, so far it is unclear whether cellular internalization of these conjugates after binding affects PIT efficacy.

The use of low molecular weight llama single domain antibodies (VHHs, nanobodies) for PIT is preferred above full size antibodies because of better tumor penetration. Therefore, we functionalized the VHH 7D12, directed against the epidermal growth factor receptor (EGFR), with a PS (IRDye700DX). To assess the impact of cellular internalization on activity, the VHHs were additionally conjugated to a cell-penetrating peptide ($VHH^{[PS]}$-CPP).

Here we show that upon illumination with near-infrared (NIR) light, both $VHH^{[PS]}$ and $VHH^{[PS]}$-CPP conjugates specifically induce cell death of EGFR expressing cancer cell lines and of EGFR-expressing cells derived from surgically obtained ascites from patients with high-grade serous ovarian cancer. However, $VHH^{[PS]}$ conjugates were significantly more effective compared to internalizing $VHH^{[PS]}$-CPP suggesting that cell surface association is required for optimal therapeutic activity.

1. Introduction

Photodynamic therapy (PDT) is a method to induce cell death through administration and activation of a photo-sensitizer (PS). When activating the PS with light of the appropriate wavelength, the PS is transferred from its ground state into an excited triplet state [1] that can return to the ground state via transmitting its energy to molecular oxygen, leading to the formation of reactive oxygen species (ROS). In general, these ROS are formed through type II photo-oxidative reactions that result in the formation of singlet oxygen, a highly toxic and short-lived radical that induces peroxidation and breakdown of lipids, proteins and nucleic acids [2].

For tumors that are amenable for local light application, PDT has a number of advantages as compared to other therapies. It is less invasive than surgery and, because of its local character, more selective than chemotherapy. Furthermore, the direct cell killing effects of PDT prevent development of resistance, as is seen with chemotherapy and most targeted therapies [3] and may also induce a vaccination effect because PDT-induced necrotic cell death releases neo-epitopes that may challenge the immune system [4]. PDT has been tested in clinical trials for cancer of the bladder, skin, head and neck. Various PSs are now approved as PDT drugs [5].

There are, however, some issues with PDT that still need to be solved. Currently used PSs suffer from low water solubility and dark toxicity. To enhance solubility, significant efforts have been made in engineering drug delivery systems that allow tumor-specific targeting of PS [6–12]. Even though antibodies are highly potent targeting vehicles, antibody-PS conjugates for photoimmunotherapy (PIT) [13,14] have the disadvantage that they circulate for weeks, increasing the risk of dark toxicity and phototoxicity in light-exposed skin [15]. To reduce

* Corresponding author at: Radboud Institute for Molecular Life Sciences, Department of Biochemistry, Geert Grooteplein 28, 6525 GA Nijmegen, The Netherlands.
E-mail address: William.Leenders@radboudumc.nl (W.P.J. Leenders).

https://doi.org/10.1016/j.ejpb.2017.12.009
Received 2 September 2017; Received in revised form 11 December 2017; Accepted 19 December 2017
Available online 20 December 2017

circulation time, conjugates of PS with small-sized recombinant llama antibodies (VHHs) have been used to induce epidermal growth factor receptor (EGFR)-dependent cell death [14,16]. The small size of these delivery systems also allows faster tumor accumulation and better tissue penetration as compared to full-size antibodies, and improves the carrier-to-drug molecular weight ratio [17].

The half-life of singlet-oxygen in biological systems is < 40 ns, restricting its toxic action radius to < 20 nm [2]. Studies using photosensitizers with different physicochemical properties that behave differently with respect to cell uptake have shown that intracellular localization greatly influences the cellular response to light-induced activation. PSs that localize to the mitochondria or cytoplasm are described to induce apoptosis, while necrosis is induced when the plasma membrane is the site of action [18,19]. Furthermore, more efficient membrane binding and membrane photooxidation increases phototoxicity of the PS [20].

Next to relying on internalization of targeted receptors, internalization of VHHs can also be triggered by conjugation to cell-penetrating peptides (CPPs) [21], a class of peptides that mediate cellular uptake of molecules that otherwise do not enter the cell [22]. Conjugation of the anti-EGFR VHH 7D12 to the CPP hLF, derived from human lactoferrin [23], endows the VHH with the capacity to enter the cell [24].

To investigate how the efficacy of PIT is influenced by the subcelullar localization of the PS we used a site-selective bioconjugation protocol to functionalize the EGFR targeting VHH 7D12 [25,26] with the PS IRDye700DX. Using sortase A transpeptidation we conjugated hLF to VHH 7D12$^{[PS]}$, yielding 7D12$^{[PS]}$-hLF. We then investigated the efficacy of both constructs on light-induced cell death and show that the CPP-free non-internalizing variant is more active in inducing cell death.

2. Material and methods

2.1. Cell culture

Human epidermoid carcinoma A431 cells, carrying an amplification of the EGFR gene [27], human high grade astrocytoma E98 cells without EGFR expression [28] and human ovarian adenocarcinoma SK-OV-3 cells with intermediate EGFR expression [29] were cultured in Dulbecco's Modified Eagle Medium (DMEM) (Lonza, Basel, Switzerland) supplemented with 10% fetal calf serum (FCS) (Gibco, Thermo Fisher Scientific, Waltham, MA, USA) and 40 μg/ml gentamycin (Centrafarm, Etten-Leur, The Netherlands). Cells were cultured at 37 °C in 5% CO_2 in a humidified atmosphere.

2.2. Sortase A expression

E. coli ER2566 cells transformed with the plasmid pGBMCS-SortA, encoding His_6-tagged sortase A with an N-terminal deletion of 59 amino acids [30] (Addgene, Cambridge, MA, USA, plasmid #21931) were grown to log phase at 37 °C, and protein expression was induced with 1.0 mM isopropyl β-D-thiogalactoside (IPTG, Serva, Heidelberg, Germany) at 30 °C for 3 h. Cells were harvested, resuspended in ice-cold 50 mM Tris pH 8.0/300 mM NaCl containing a protease inhibitor cocktail (Roche, Basel, Switzerland) and lysed by sonication using a Bandelin Sonopuls HD2070 sonicator (Bandelin electronic GmbH & Co, Berlin, Germany). After centrifugation the supernatant was incubated with Ni-NTA sepharose (IBA, Goettingen, Germany) in 50 mM phosphate pH 7.4/500 mM NaCl for 1 h at 4 °C. After washing, His_6-tagged sortase A was eluted from the beads with 500 mM imidazole. The eluate was dialyzed against 50 mM Tris pH 7.5/150 mM NaCl in a 3.5 kDa dialysis membrane (Spectrum Labs, Los Angeles, CA, USA). Protein purity was analyzed by SDS-PAGE gel electrophoresis under reducing conditions and liquid chromatography mass spectrometry (LC–MS, Shimadzu HPLC and Thermo Finnigan LCQ Fleet) on a C4 column. Protein concentration was determined by absorbance at 280 nm using the Nanodrop spectrophotometer (LI-COR, Lincoln, NE, USA).

2.3. VHH expression

The cDNA encoding anti-EGFR VHH 7D12 (a gift from Paul van Bergen en Henegouwen, Utrecht University, The Netherlands) was recloned into the vector pHENIX-C-LPETG-His_8-Vsv, resulting in 7D12-C-LPETG-His_8-Vsv, the cysteine providing a handle for maleimide conjugation, LPETG being a sortase A consensus recognition sequence and the His_8-Vsv tag allowing Ni-based purification and Vsv-based detection. 7D12-C-LPETG-His_8-Vsv expression was induced via standard methods in *E. coli* strain TG1. Cells were harvested by centrifugation at 2830*g* for 20 min at 4 °C, resuspended in ice cold Tris/EDTA/sucrose (TES) buffer (200 mM Tris pH 8.0/0.5 mM EDTA/20% w/v sucrose/protease inhibitor cocktail) and incubated for 20 min on ice, followed by centrifugation (4424*g*, 20 min, 4 °C). The supernatant was collected and the pellet was resuspended in TES buffer supplemented with 15 mM $MgSO_4$, and incubated on ice for 20 min. After centrifugation, both supernatants were pooled and protein was purified with Ni-NTA sepharose as described for sortase A.

2.4. IRDye700DX conjugation

All steps involving IRDye700DX were performed in the dark. 7D12-C-LPETG-His_8-Vsv was incubated with 20 mM tris(2-carboxyethyl) phosphine (TCEP) (Thermo Fisher Scientific, Waltham, MA, USA) for 15 min at room temperature to reduce the free thiol group of the cysteine. TCEP was removed in a 10 kDa MWCO centrifugal unit (Amicon, Millipore, Billerica, MS, USA) employing 5 washing cycles with 20 mM phosphate pH 7.0/150 mM NaCl/5 mM EDTA. Maleimide-PEG_4-DBCO (Jena Bioscience, Jena, Germany, 10 mM stock in DMF) was allowed to react for 2 h at room temperature in a thermoshaker at 450 rpm with 7D12-C-LPETG-His_8-Vsv in a 3:1 molar ratio, yielding 7D12-C$^{[DBCO]}$-LPETG-His_8-Vsv. Excess maleimide-PEG_4-DBCO was removed by filter centrifugation in a 10 kDa MWCO centrifugal unit employing 4 washing cycles with 50 mM Tris pH 7.5/150 mM NaCl. The protein conjugate was analyzed by LC–MS, and protein concentration was determined by ultraviolet absorbance at 309 nm using the Nanodrop spectrophotometer.

In parallel, IRDye700DX-NHS (LI-COR, Lincoln, NE, USA from now on referred to as PS-NHS) was incubated with H_2N-PEG_3-N_3 (Jena Bioscience, Jena, Germany) in a 3:1 molar ratio in 100 mM phosphate buffer pH 8.6/150 mM NaCl for 7 h at RT in a thermoshaker at 450 rpm, yielding PS-N_3. Subsequently 7D12-C$^{[DBCO]}$-LPETG-His_8-Vsv was incubated with PS-N_3 in a 1:2 molar ratio o/n at RT in a thermoshaker at 450 rpm, yielding 7D12-C$^{[PS]}$-LPETG-His_8-Vsv. This conjugate was purified from unconjugated PS-N_3 by centrifugation in a 10 kDa MWCO centrifugal unit employing 4 washing cycles with 50 mM Tris pH 7.5/150 mM NaCl. The protein was analyzed by SDS-PAGE gel electrophoresis under reducing conditions and with electrospray ionization time-of-flight mass spectrometry (ESI-ToF) on a JEOL AccuTOF-CS (JEOL, Tokio, Japan). Protein concentration was determined by measuring absorbance at 689 nm (ε = 165,000 M^{-1} cm^{-1}, assuming 1:1 complete labeling) using the Nanodrop spectrophotometer.

2.5. Functionalization of 7D12-C$^{[PS]}$-LPETG-His_8-Vsv with hLF

GGG-hLF or GGG-hLF$^{(Fluo)}$ (synthesized by EMC microcollections, Tübingen, Germany) was dissolved in 50 mM HEPES pH 8.0 at 5–10 mM, to ensure intramolecular disulfide bridge formation that is required for CPP activity [31]. The carboxyfluorescein moiety was coupled to a C-terminal lysine residue. Subsequently sortase A (80 μM final concentration) and GGG-hLF (100 μM final concentration) were added to 7D12-C$^{[PS]}$-LPETG-His_8-Vsv (20 μM final concentration) in 50 mM Tris pH 7.5/150 mM NaCl/10 mM $CaCl_2$. The sortase reaction was allowed to proceed for 5 h at 30 °C in a thermoshaker at 450 rpm,

after which the reaction mixture was incubated with pre-washed Ni-NTA sepharose beads to remove the His_6-tagged sortase A, G-His_8-Vsv and unreacted 7D12-$C^{[PS]}$-LPETG-His_8-Vsv. Excess GGG-hLF was removed from the Ni-NTA agarose supernatant by filtration in a 10 KDa MWCO centrifugal unit employing 6 cycles against 20 mM phosphate pH 7.5/500 mM NaCl. Purity and concentration of the VHH conjugate were analyzed by SDS-PAGE gel electrophoresis and ESI-ToF. Protein concentrations were determined by measuring absorbance at 689 nm using the Nanodrop spectrophotometer.

2.6. Fluorescein labeled constructs for confocal microscopy applications

For confocal microscopy applications, 7D12 constructs directly labeled with fluorescein were produced. 7D12-C-LPETG-His_8-Vsv was reduced with 20 mM TCEP as described above. Then fluorescein-5-maleimide (Thermo Fisher Scientific, Waltham, MA, USA, 10 mM stock in DMF) was reacted with reduced 7D12-C-LPETG-His_8-Vsv in a 3:1 molar ratio in 20 mM phosphate pH 7.0/150 mM NaCl/5 mM EDTA for 2 h at RT in a thermoshaker at 450 rpm. Excess fluorescein-5-maleimide was removed by filtration in a 10 kDa MWCO centrifugal unit employing 4 washing cycles with 50 mM Tris pH 7.5/150 mM NaCl. 7D12-C-LPETGGG-$hLF^{[Fluo]}$ was prepared using sortase A as described above, using 50 μM sortase A, 50 μM GGG-$hLF^{[Fluo]}$ and 20 μM 7D12-C-LPETG-His_8-Vsv in 50 mM Tris pH 7.5/150 mM NaCl/10 mM $CaCl_2$. The product was purified using Ni-NTA sepharose and filter centrifugation as described. Protein conjugates were analyzed by SDS PAGE gel electrophoresis under reducing conditions and LC-MS. Protein concentration was determined by measuring absorbance at 494 nm ($\varepsilon = 75{,}000\ M^{-1}\ cm^{-1}$, assuming 1:1 complete labeling) using the Nanodrop spectrophotometer.

2.7. Cell uptake assays with confocal microscopy

Cellular uptake of the different fluorescein-labeled 7D12 conjugates was examined with confocal microscopy on a TCS SP5 microscope (Leica Microsystems, Mannheim, Germany) equipped with an HCX PL APO 63 × 1.2 water immersion lens. During imaging, cells were maintained at 37 °C. The 488 nm laser line of the argon laser was used for excitation and emission was collected between 500 and 550 nm. A431, E98 and SK-OV-3 cells (30,000, 50,000 and 30,000 cells per well, respectively) were plated in 8-well Lab-Tek borosilicate coverglass chambers (NUNC, Thermo Fisher Scientific, Waltham, MA, USA) and allowed to adhere and proliferate for 48 h. Then cells were incubated for 30 min at standard culture conditions in 200 μl phenol red-free RPMI/10% FCS, supplemented with 2 μM of 7D12-$C^{[Fluo]}$-LPETG-His_8-Vsv, 7D12-C-LPETGGG-$hLF^{[Fluo]}$, or GGG-$hLF^{[Fluo]}$. Subsequently, cells were washed twice with phenol red-free RPMI/10% FCS containing 20 mM HEPES and were imaged by confocal microscopy. Acidic pH in lysosomes reduces fluorescein fluorescence. To investigate if this effect lead to an underestimation of 7D12-$hLF^{[Fluo]}$ uptake, we treated cells with 65 μM chloroquine, which increases the lysosomal pH and thereby enhances fluorescein fluorescence [32]. The samples were imaged once more and, to quench extracellular fluorescence, 0.4% trypan blue (Sigma Aldrich, Saint Louis, MO, USA) was added to the wells before imaging for a third time [33].

2.8. Study of cell uptake mechanism with confocal microscopy

To detect clathrin-dependent endocytosis, cells were co-incubated with the constructs as described above and 100 μg/ml transferrin-Alexa Fluor 633 (Life Technologies, Thermo Fisher Scientific, Waltham, MA, USA). After 30 min, the cells were washed and colocalization of transferrin and the constructs was detected by confocal microscopy. Fluorescein was excited with the argon laser at 488 nm and emission was detected between 500 and 550 nm. Alexa Fluor 633 was excited with the 633 nm helium-neon laser and fluorescence detected between 650 and 715 nm.

2.9. In vitro PDT assays with adherent cell cultures

A431, E98 and SK-OV-3 cells were cultured in clear 96-well plates (Costar, Greiner-Bio One, Essen, Germany). At 80% confluency cells were incubated for 30 min with different concentrations of 7D12-$C^{[PS]}$-LPETG-His_8-Vsv, 7D12-$C^{[PS]}$-LPETGGG-hLF or equimolar concentrations of PS alone in DMEM/10% FCS. Controls were incubated with DMEM/10% FCS only. Cells were washed twice with warm DMEM/10% FCS. Immediately after washing, plates were illuminated with 100 mW/cm^2 for 600 s, reaching a total light dose of 60 J/m^2, using a standardized light emitting diode device (690 ± 10 nm) as described in [34]. To determine dark toxicity, cells were incubated with the highest used concentration of the conjugates without subsequent illumination. After overnight incubation a sulforhodamine-B-assays (SRB) assay was performed as described in [35] to determine total protein content. Results were expressed as cell viability relative to controls (untreated illuminated cells). Half maximal inhibitory concentration (IC50) of the various conjugates were determined in GraphPad Prism 5.02 (LaJolla, CA, USA).

To examine selectivity of PDT-induced cytotoxicity with the different conjugates, 5×10^5 cells were labeled with DiO (A431 and SK-OV-3) or DID (E98) dye (Life technologies, Thermo Fisher Scientific, Waltham, MA, USA) according to manufacturers protocol. Mixtures of A431, E98 and SK-OV-3 cells were plated and subjected to PDT as described above. Immediately, 2 h and 16 h after illumination cells were incubated with 1 μg/ml propidium iodide (Thermo Fisher Scientific, Waltham, MA, USA) in PBS for 15 min. Cells were visualized with the EVOS FL digital inverted fluorescence microscope (Thermo Fisher Scientific, Waltham, MA, USA) using the RFP LED light cube (Propidium Iodide), the GFP LED light cube (DiO labeled cells) and the Cy5 LED light cube (DiD labeled cells).

2.10. Mechanism of cell death

To check if apoptotic cell death was induced by 7D12-$C^{[PS]}$ conjugates, cells were treated with 15 nM 7D12-$C^{[PS]}$ conjugates and illuminated as described. Immediately, 2 h and 20 h after illumination cells were incubated with 1:250 Annexin-V-Alexa488 (Life Technologies, Thermo Fisher Scientific, Waltham, MA, USA) and 1 μg/ml propidium iodide in 10 mM HEPES pH 7.4/140 mM NaCl/2.5 mM $CaCl_2$ to stain apoptotic and dead cells, respectively. Stained cells were visualized with the EVOS. As a positive control, cells were treated with 2 μM staurosporin for 4 h at 37 °C

Furthermore, extracts of treated cells 2 h and 4 h after illumination and of staurosporin-treated control cells were made with RIPA buffer (#9806, Cell Signaling Technology, Danvers, MA, USA). 20 μg of total protein was run on an 8% SDS-PAGE gel, and electroblotted on a nitrocellulose membrane (GE healthcare, Little Chalfont, USA). Blots were stained with rabbit-anti-cleaved-Caspase-3 (Asp175) (1:1000, #9661, Cell Signaling Technology, Danvers, MA, USA) and mouse-anti-GAPDH. Blots were visualized on the Odyssey scanner.

2.11. In vitro PDT assays with spheroids

Because 3D cell cultures better recapitulate clinical tumors than adherent 2D cell cultures, we grew SK-OV-3 cells as tumor spheroids. To this end, 96-well round bottom culture plates were coated with 100 μl/well 1% agarose (Sigma Aldrich, Saint Louis, MO, USA) in DMEM/F12 medium (Gibco, Thermo Fisher Scientific, Waltham, MA, USA). SK-OV-3 cells (30,000/well) were seeded in 100 μl DMEM/F12 medium containing 0.3% BSA. Three days after seeding, the spheres were incubated for 30 min or 1 h at 37 °C in DMEM/10% FCS and 120 nM 7D12-$C^{[PS]}$-LPETG-His_8-Vsv, 7D12-$C^{[PS]}$-LPETGGG-hLF, PS alone or medium only. After washing with DMEM/10% FCS spheres

were illuminated with a 60 J/m^2 total light dose. After overnight incubation at 37 °C, spheres were fixed in Unifix (Klinipath, Duiven, The Netherlands) at RT, and embedded in agar. 4 μM sections were stained with hematoxylin and eosin.

2.12. Ex vivo PDT assays with clinical ascites samples

All experiments with patient materials were performed according to institutional guide lines. To examine whether PIT with our conjugates could be an option for treatment of ovarian cancer we tested our constructs on cells, freshly derived from malignant ascites of patients diagnosed with high-grade serous ovarian carcinoma. Ascites was filtered through a 70 μm cell strainer. Nucleated cells were isolated by centrifugation on Ficoll, according to the manufacturer's instructions (Sigma Aldrich, Saint Louis, MO, USA) and cultured in RPMI/10% FCS/40 μg/ml gentamycin. For PDT experiments, cells were seeded at 10,000 cells per well in a 96-well plate and grown until > 50% confluency. After incubation with 15 nM of 7D12-C$^{[PS]}$-LPETG-His$_8$-Vsv, 7D12-C$^{[PS]}$-LPETGGG-hLF or PS alone for 30 min, cells were illuminated with 60 J/m^2 total light dose. The next day, cell viability was determined using the SRB assay. In parallel experiments, ascites-derived cells were incubated with 15 nM of the different 7D12-C$^{[PS]}$ conjugates for 30 min, illuminated and incubated overnight. The next day, cells were incubated with either 1 μg/ml cetuximab for 20 min and goat-anti-human Alexa488 (1:200 Thermo Fisher Scientific, Waltham, MA, USA) for 20 min to verify EGFR expression, or mouse-anti-EpCAM (1:200 Abcam, Cambridge, UK ab7504) and donkey-anti-mouse Alexa488 (1:200 Thermo Fisher Scientific, Waltham, MA, USA) to verify EpCAM expression, and with 1 μg/ml propidium iodide (Thermo Fisher Scientific, Waltham, MA, USA) to visualize the dead cells. Propidium iodide and bound antibodies were visualized using the EVOS microscope.

2.13. Statistics

Experiments were performed at least in duplicate, and within experiments all measurements were done in triplicate. IC50 values were determined in Graphpad Prism and statistical significance was checked with a Student's T-test. To check for significance of other data a one-way ANOVA with post hoc Bonferroni was performed in Graphpad Prism; * = $p < .05$, ** = $p < .01$, *** = $p < .001$.

3. Results and discussion

3.1. Preparation and characterization of 7D12-C$^{[PS]}$ conjugates

Targeted PDT of cancers requires high tumor selectivity and specificity, concomitant with a lack of dark toxicity. Approaches that improve tumor selectivity of the PS by conjugation to antibodies still have major drawbacks due to the long circulation half-lives of these conjugates, and poor penetration of these large constructs into poorly perfused tumor areas. To tackle these problems, smaller targeting moieties like VHHs are interesting alternative PS carriers. Here, the anti-EGFR VHH 7D12 was used as a clinically relevant model VHH to examine how subcellular localization of PSs affects PDT efficacy. It was published before that 7D12-IRdye700DX conjugates can be prepared successfully via NHS-based conjugation to lysines [14]. This approach however, carries a risk of overlabeling of lysines that are involved in antigen binding, resulting in reduced affinity. Also, this procedure yields a heterogeneous mixture of VHHs, containing a fraction of unlabeled VHHs that may act as competitor for the labeled ones. We therefore chose to perform a site-selective reaction at an introduced cysteine at the carboxyterminus (Fig. 1A). Because IRDye700DX was not available as a maleimide conjugate at the time of this study, we first coupled a dibenzocyclo-octyn (DBCO)-functionality to the VHH and an azide functionality to the PS. This enabled us to use the highly specific and bio-orthogonal click reaction between azide and DBCO [36]. 7D12-C$^{[DBCO]}$-LPETG-His$_8$-Vsv and 7D12-C$^{[PS]}$-LPETG-His$_8$-Vsv were produced successfully as verified with SDS-PAGE electrophoresis (Fig. 1B) and LC-MS (Fig. 1C). LC-MS verified conjugation of only one maleimide-DBCO and PS molecule per VHH, as we have seen before for maleimide-fluorescein [37]. This method is generally applicable to all VHHs, as long as these do not carry unpaired cysteines in the complementarity determining region, and since all reactions occur distant from the VHHs' antigen binding site, this approach is predicted to retain VHH affinity.

By employing sortase-A-mediated ligation of GGG-hLF (Fig. 1D), we successfully produced 7D12-C$^{[PS]}$-LPETGGG-hLF (Fig. 1B and E). Because we did not have lasers compatible for detection of IRDye700DX–fluorescence with confocal microscopy, we also prepared fluorescein labeled variants 7D12-C$^{[Fluo]}$-LPETG-His$_8$-Vsv and 7D12-C-LPETGGG-hLF$^{[Fluo]}$.

3.2. Cellular binding and uptake of 7D12 conjugates

Previous research has shown that hLF is taken up by endocytosis at concentrations below 10 μM [23], and that functionalization of 7D12 with hLF causes increased internalization of the VHH [24]. Here we confirmed these patterns of cellular uptake in A431 and SK-OV-3 cells (Fig. 2). Cells were incubated with the conjugates at a concentration of 2 μM at which little vesicular uptake of hLF alone was observed (supplementary Fig. 1A). 7D12-C$^{[Fluo]}$-LPETG-His$_8$-Vsv showed a predominant membrane staining whereas for 7D12-C-LPETGGG-hLF$^{[Fluo]}$ membrane staining was weaker and a more pronounced vesicular fluorescence was observed. SK-OV-3 cells showed very weak membrane staining after incubation with 7D12-C$^{[Fluo]}$-LPETG-His$_8$-Vsv, but after incubation with 7D12-C-LPETGGG-hLF$^{[Fluo]}$ intracellular vesicular staining was observed, which was more clearly visible after quenching extracellular fluorescence with trypan blue (Fig. 2). No binding to or uptake in E98 was observed for both 7D12 conjugates (supplementary Fig. 1B). This latter finding further confirmed that cell association was primarily VHH and not hLF driven.

It is generally accepted that CPPs lack cell line selectivity, however, such experiments are typically conducted at medium micromolar concentrations [38]. The dissociation constant of the binding of hLF to cell surface glycosaminoglycans is in the low micromolar range [31], while reported Kd values of 7D12 binding to cell-associated EGFR is in the order of 10–20 nM [14,17,26]. Cell ELISAs, performed at 4 °C to study binding in the absence of internalization, confirmed high affinity binding of 7D12-C$^{[PS]}$-LPETG-His$_8$-Vsv and 7D12-C$^{[PS]}$-LPETGGG-hLF to EGFR overexpressing A431 cells (Kd = 11.85 ± 1.203 and 25.53 ± 2.514 nM, respectively; not shown). At the low micromolar and subnanomolar concentrations that we employed in the uptake and PDT assays, respectively, binding of the different conjugates is therefore expected to be determined by the 7D12 moiety, rather than hLF. This finding has important implications for *in vivo* applications of CPP-based strategies. Except for those tissues that show a high propensity for CPP uptake [39], uptake of VHH-CPP conjugates is directed by the presence of EGFR. In this case, the CPP module is a modulator of subcellular trafficking rather than an unspecific driver of uptake.

3.3. hLF mediated uptake of 7D12 is initiated by clathrin mediated endocytosis

In previous work we showed that 7D12-LPETGGG-hLF$^{[Fluo]}$ induces internalization of EGFR [24], which can be initiated by clathrin mediated endocytosis (CME) and/or clathrin independent endocytosis [40]. To investigate if the 7D12-LPETGGG-hLF$^{[Fluo]}$ induced internalization of EGFR is clathrin-dependent we incubated A431 cells with the various CPP constructs in the presence of transferrin-Alexa633 (Fig. 3). Both 7D12-LPETGGG-hLF$^{[Fluo]}$ and hLF$^{[Fluo]}$ but not 7D12$^{[Fluo]}$-LPETG-His$_8$-Vsv induced vesicular uptake as seen by enhanced transferrin staining

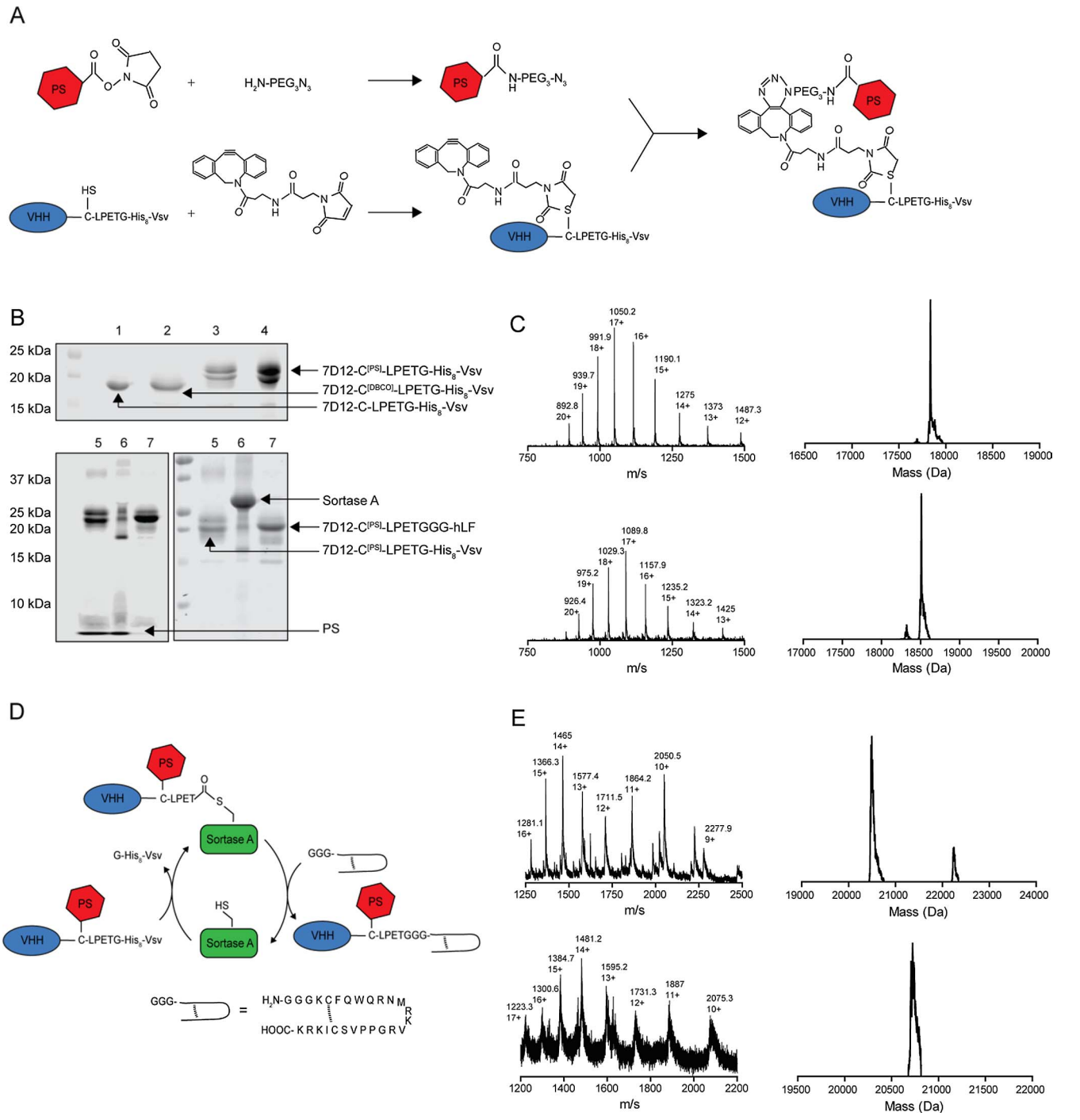

Fig. 1. Analytical characterization of the conjugates. (A) Scheme of bio-orthogonal conjugation of azide-functionalized PS to the DBCO-functionalized VHH. (B) Upper panel: coomassie brilliant blue (CBB) stained SDS-PAGE gel of the reaction products after conjugation of the N_3-PEG_3-PS to 7D12-$C^{[DBCO]}$-LPETG-His_8-Vsv (1: 7D12-C-LPETG-His_8-Vsv, 2: 7D12-$C^{[DBCO]}$-LPETG-His_8-Vsv, 3: 7D12-$C^{[PS]}$-LPETG-His_8-Vsv before column purification, 4: 7D12-$C^{[PS]}$-LPETG-His_8-Vsv after column purification). Lower panel: visualization of the SDS-page gel at 680 nm before coomassie staining (left) and of the coomassie-stained gel (right) with reaction products and controls of the sortase A conjugation to functionalize 7D12-$C^{[PS]}$-LPETG-His_8-Vsv with GGG-hLF (5: 7D12-$C^{[PS]}$-LPETG-His_8-Vsv, 6: Sortase A /7D12-$C^{[PS]}$-LPETG-His_8-Vsv after 5 h incubation at 30 °C, 7: the final product 7D12-$C^{[PS]}$-LPETGGG-hLF after Ni-NTA purification). (C) LC-MS characterization of TCEP-reduced 7D12-C-LPETG-His_8-Vsv (upper, observed 17,837 Da, calculated 17837.6 Da) and 7D12-$C^{[DBCO]}$-LPETG-His_8-Vsv (lower, observed 18,511 Da, calculated 18512.4 Da). The left graphs show the total mass spectra, the right graphs show the deconvoluted spectra. (D) Scheme of site specific conjugation of VHH-$C^{[PS]}$-LPETG-His_8-Vsv to GGG-hLF with sortase A. (E) ESI-ToF characterization of 7D12-$C^{[PS]}$-LPETG-His_8-Vsv (upper graphs, observed 20,495 Da, calculated 20569.7 Da) and 7D12-$C^{[PS]}$-LPETGGG-hLF (lower graphs, observed 20,724 Da, calculated 20720.2 Da). The left graphs show the total mass spectra, the right graphs the deconvoluted spectra.

that colocalized with the hLF-containing constructs.

3.4. PIT efficacy of 7D12-$C^{[PS]}$ constructs in adherent cell cultures

Cell killing assays showed that 7D12-$C^{[PS]}$ conjugates were very potent and specific PDT agents, without inducing dark toxicity (Fig. 4A and C). Incubation with PS alone, followed by illumination did not induce cell killing under the conditions used (Fig. 4B). Although the 7D12-$C^{[PS]}$ conjugates that we produced via a two-step click reaction contained only one PS per VHH, these induced EGFR-specific cell death very efficiently, with an IC50 value for 7D12-$C^{[PS]}$-LPETG-His_8-Vsv on A431 cells of 87.8 ± 4.3 pM after NIR light illumination with 60 J/m^2.

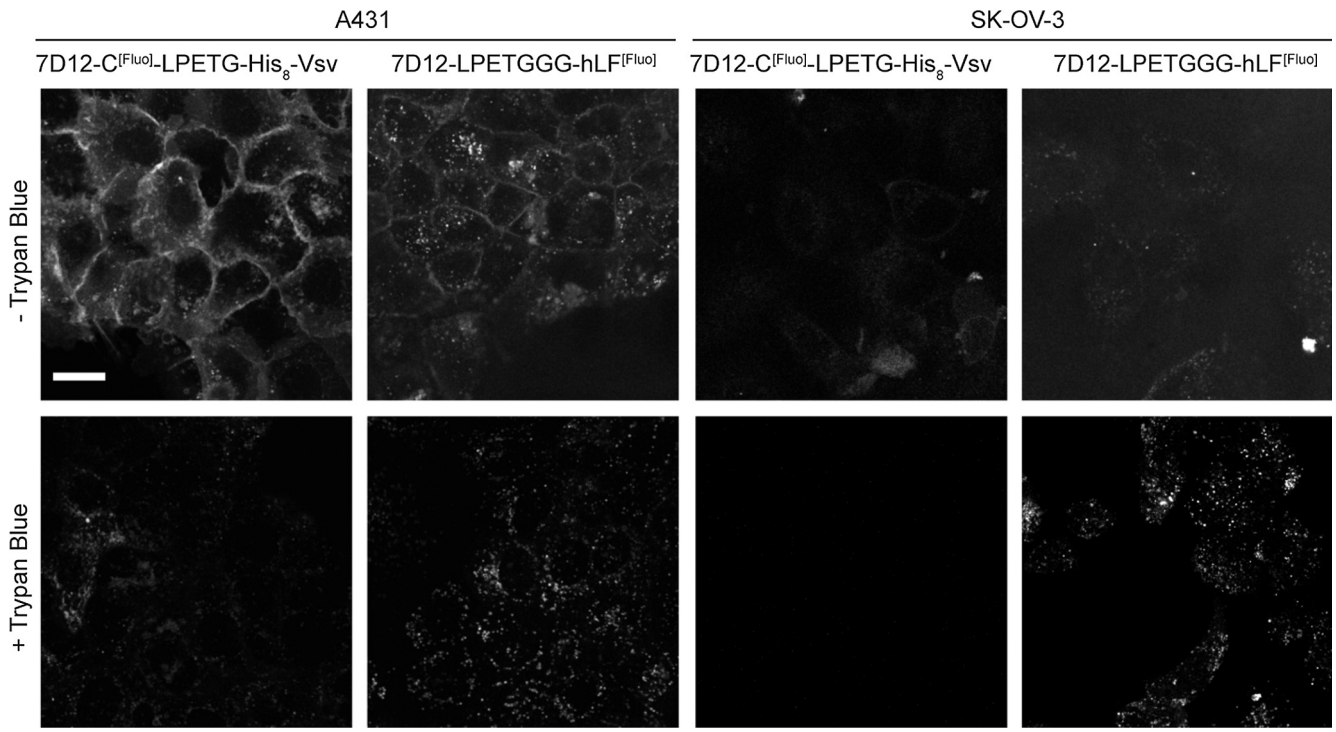

Fig. 2. Cell binding and uptake of the constructs. A431 and SK-OV-3 cells were incubated with 2 μM of 7D12-C$^{[Fluo]}$-LPETG-His$_8$-Vsv and 7D12-C-LPETGGG-hLF$^{[Fluo]}$ and imaged by confocal laser scanning microscopy before and after quenching fluorescence from extracellular located fluorescein with trypan blue (TB). The scale bar denotes 10 μm.

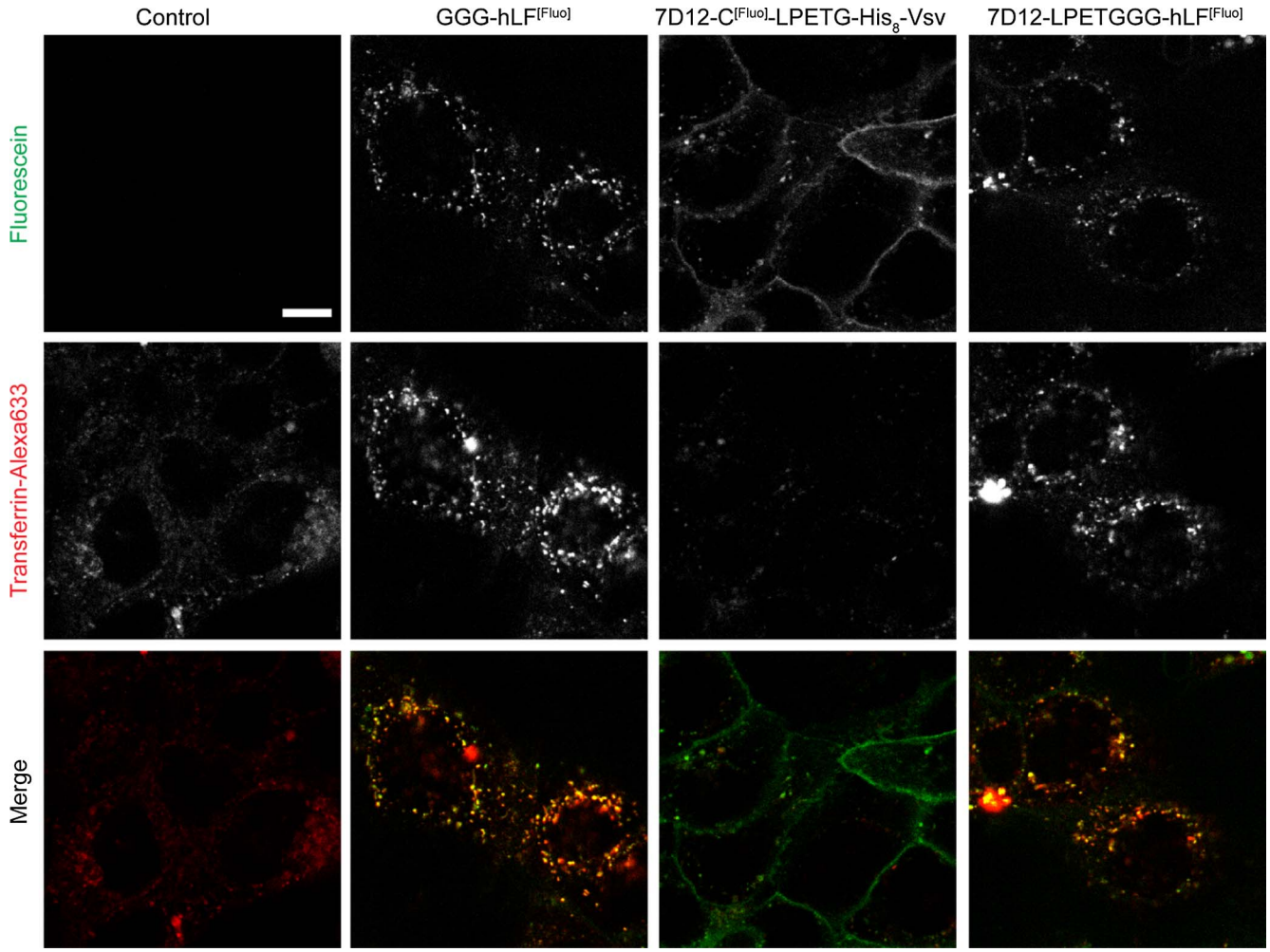

Fig. 3. Induction of clathrin-dependent endocytosis by hLF conjugates. A431 cells were incubated for 30 min with 2 μM of the CPP constructs in the presence of transferrin-Alexa633. The scale bar denotes 10 μm.

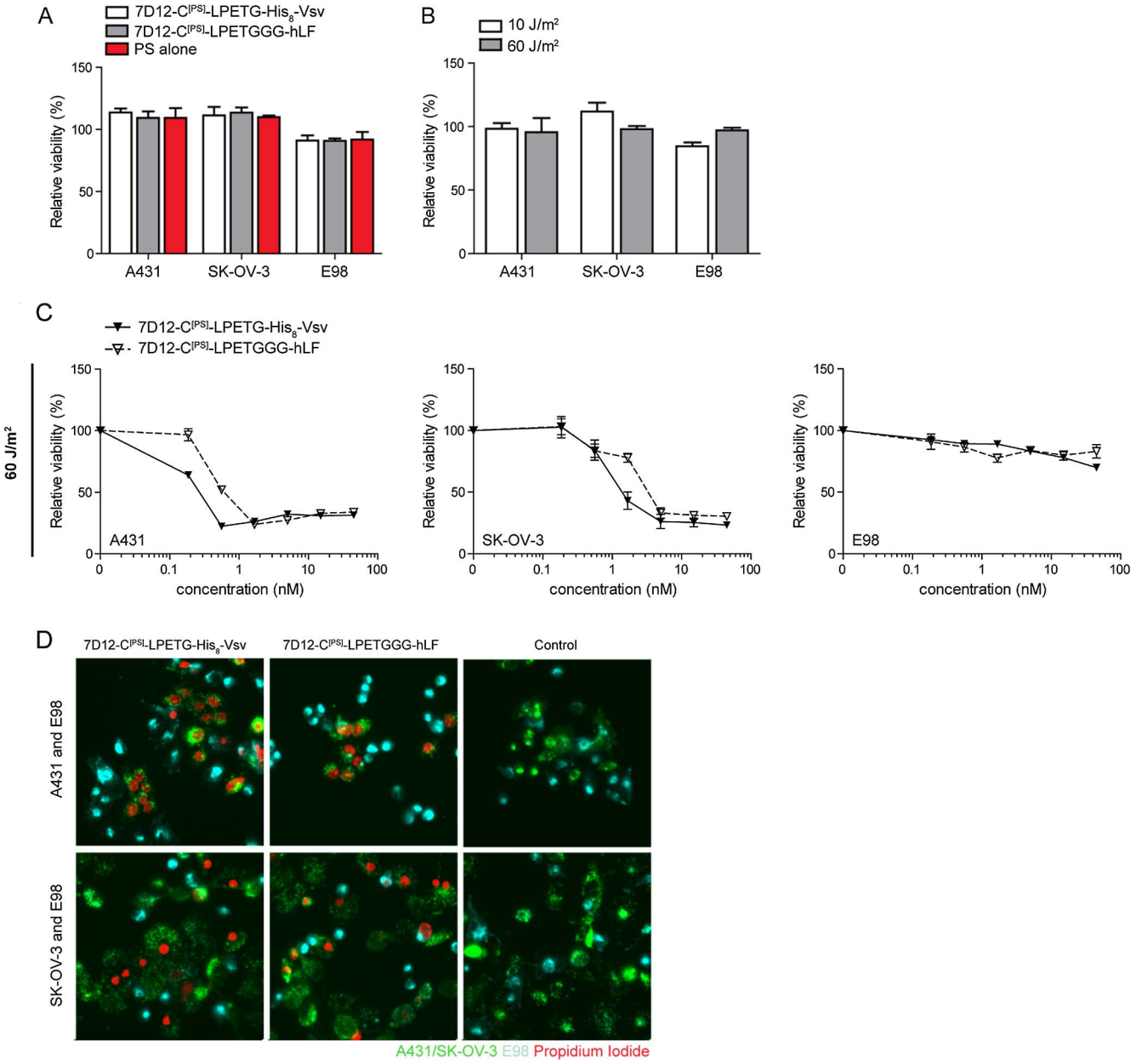

Fig. 4. Phototoxicity induced by the constructs in adherent cells. (A) Absence of dark toxicity of 7D12-C$^{[PS]}$ constructs (45 nM) and PS alone (45 nM for 10 J/m^2 and 15 nM for 60 J/m^2) and (B) toxicity of non-targeted PS with illumination. Results are shown as survival relative to untreated cells. (C) The relative cell viability after incubation with various concentrations of 7D12-C$^{[PS]}$ constructs and illumination with a 60 J/m^2 total light dose was also determined in SRB assays. (D) Co-cultures fluorescently labeled with DiDyes were incubated with 15 nM 7D12-C$^{[PS]}$ constructs and illuminated with a 60 J/m^2 total NIR light dose. Two hours after illumination cells were imaged. Controls were illuminated only.

Interestingly, conjugates containing hLF were less effective with an IC50 of 234.1 ± 122.7 pM (p = .3556) (Fig. 4C). In the intermediate EGFR expressing SK-OV-3 cells, similar differences were observed between 7D12-C$^{[PS]}$-LPETG-His$_8$-Vsv (IC50 = 705.1 ± 164 pM) and the internalizing variant 7D12-C$^{[PS]}$-LPETGGG-hLF (IC50 = 2680 ± 323.5 pM) (p = .0055). Interestingly, in previous reports it was demonstrated that VHH-PS conjugates with higher affinity for EGFR had higher PIT efficacy and it was suggested that increased internalization due to higher affinity was responsible for increased photosensitivity [14]. Furthermore, internalizing antibody-PS conjugates were shown to be more effective in PIT than non-internalizing antibody-PS [41]. Our data, however, show that increased cell surface association is a more important determinant. Interestingly, no phototoxicity was induced in non-EGFR expressing E98 cells in line with the low cell binding capacity mediated by the CPP alone.

To further assess the selectivity of the 7D12-C$^{[PS]}$ conjugates, co-culture experiments with A431, E98 and SK-OV-3 were performed. These cell types were distinguished by pre-labeling them with different membrane associated dyes. Labeled and dead cells were visualized immediately, 2 h and 16 h after illumination (Fig. 4D and supplementary Fig. 2). Only EGFR expressing cells were killed after PDT (Fig. 4D). No cell death was observed in the controls (no PS-conjugates added, data not shown). Parallel experiments with monocultures of the cells showed that cell death was induced immediately after illumination for the A431 cells, and after 2–16 h for the SK-OV-3 cells (supplementary Fig. 3). The cell death of A431 immediately after PDT suggested that necrosis was induced. Neither A431 and SK-OV-3 cells were stained with Annexin-V (not shown), and they did not induce caspase-3 dependent apoptosis at 4 h after PDT, which further indicates that cells indeed died by necrosis (supplementary Fig. 4). Unconjugated IRDye700DX did not lead to phototoxicity in all used cell types, in agreement with previous studies, and did not display dark toxicity. This

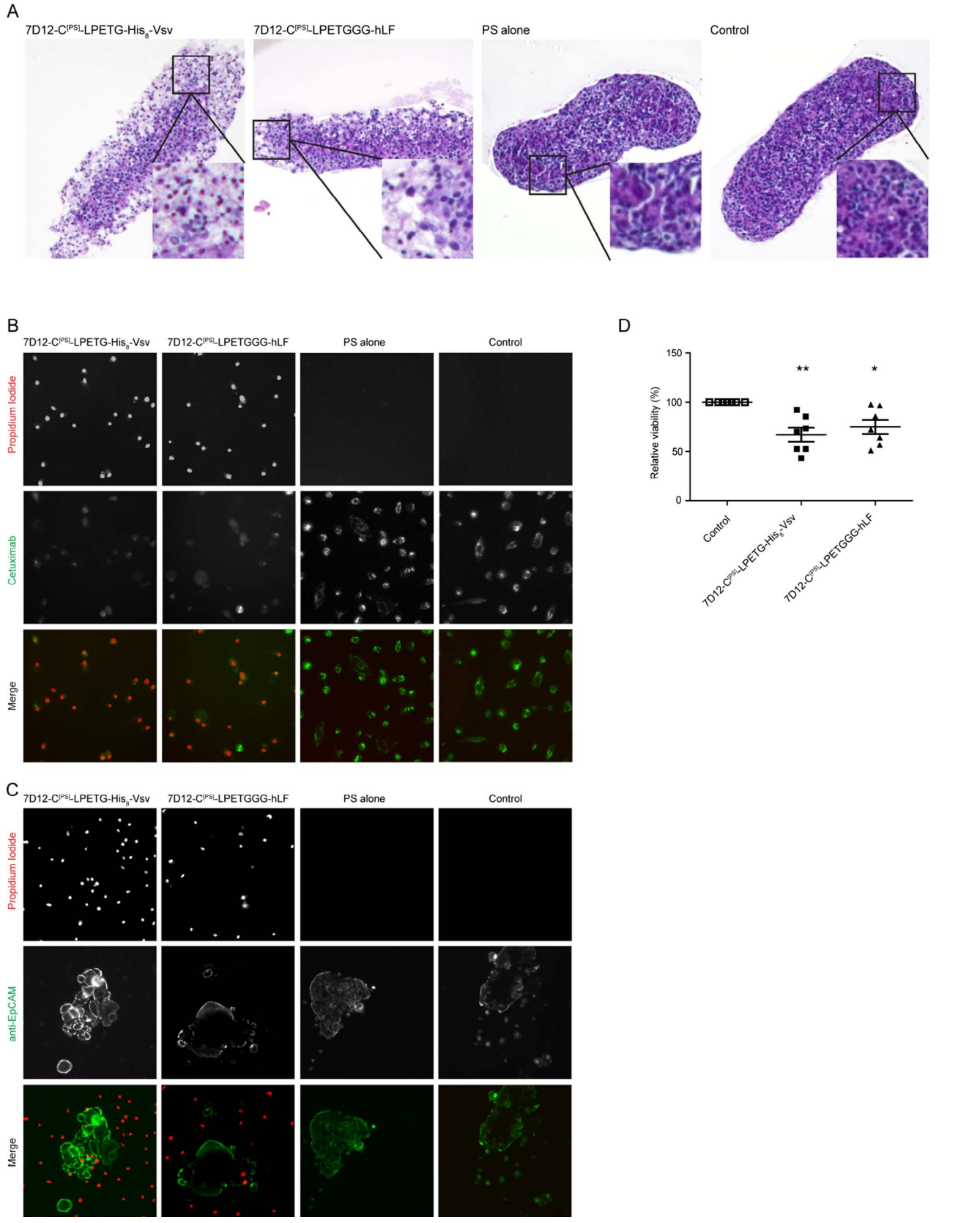

Fig. 5. Phototoxicity induced by the constructs in ovarian carcinoma spheroids and clinical ascites. (A) SK-OV-3 spheres were incubated with 120 nM of the 7D12-C$^{[PS]}$ constructs or controls and illuminated with a NIR light dose of 60 J/m^2. Sections of agar-embedded treated or control SK-OV-3 spheroids were stained with hematoxylin and eosin. Note that the outer layer of cells have picnotic nuclei, visualized more clearly in the enlarged insert. (B + C) Cultured cells from clinical ascites were incubated with 15 nM of the various 7D12-C$^{[PS]}$ constructs and illuminated with a total NIR light dose of 60 J/m^2. Dead cells and (B) EGFR or (C) EpCAM expressing cells in an ascites derived cell culture after PDT were imaged. Note the weaker signal of cetuximab in the dead 7D12-C$^{[PS]}$ treated samples compared to the live cells in the controls. (D) The percentage of cell viability in multiple cultures was determined with SRB assays. * = $p < .05$, ** = $p < .01$.

makes it a suitable compound for targeted PDT [42].

3.5. Efficient PIT with ovarian carcinoma SK-OV-3 spheroids and EGFR positive cells in clinical ascites

To assess effectiveness of the conjugates in a cellular model with more resemblance to the *in vivo* tumor situation, conjugates were incubated with SK-OV-3 spheroids. PIT with SK-OV-3 spheroids showed efficient cell killing after incubation with 120 nM of the 7D12-$C^{[PS]}$-LPETG-His_8-Vsv construct and a light dose of 60 J/m^2, illustrated by the majority of cells with picnotic nuclei in the HE stained sections, and only a minority of cells in the centre that appeared viable (Fig. 5A, enlargement in insert). In the 7D12-$C^{[PS]}$-LPETGGG-hLF treated cells, also dead cells with picnotic nuclei were observed but to a lesser extent. Control spheres showed only viable cells, indicating that cell death also in the centre is due to penetration of the VHH conjugates into the spheroid.

Finally, cells derived from clinical ascites from women with stage III or IV high-grade serous ovarian carcinoma (n = 7) were incubated with 15 nM 7D12-$C^{[PS]}$ constructs and illuminated with 60 J/m^2 NIR light. Phototoxicity was restricted to the EGFR-positive subpopulation of cells, as could be observed by costainings for dead cells (propidium iodide) and EGFR (Cetuximab). The absence of costaining for dead cells and a population of cells positive for another tumor marker (EpCAM) indicated selectivity for EGFR (Fig. 5C). SRB assays after incubation with 7D12$^{[PS]}$ constructs and illumination showed significant decreases in overall cell viability compared to controls ($P < .001$ and $P < .03$ for 7D12-$C^{[PS]}$-LPETG-His_8-Vsv and 7D12-$C^{[PS]}$-LPETGGG-hLF, respectively (Fig. 5D). The survival of about 60–70% of the cells is in agreement with the notion that ascites also contain numerous non-EGFR-expressing cells (as shown in Fig. 5C) that are expected to survive the treatment.

With the use of optical fibers NIR light can be delivered to otherwise inaccessible tumors, as has been shown for peritoneal metastasis of ovarian cancer using Verteporfin [43]. In addition, peroperative fluorescent image-guided surgery is gaining momentum [44] and could be very well extended with compounds comparable to those described here.

4. Conclusion

Targeted PDT is a rapidly increasing field which promises to become of great importance for the treatment of light-accessible malignancies. Targeted light-induced cancer cell death has great advantages as compared to currently applied targeted treatments which mostly only delay progression of cancers, giving these ample time to develop resistance. We here describe the construction of a highly defined VHH-PS via a controlled bioconjugation method that is easily applicable to other VHHs. Despite the fact that every VHH carries only one PS molecule, these constructs are highly selective and specific, requiring very low concentrations to induce efficient cell killing via necrosis. In 3D-spheroid models, efficient cell killing was observed, indicating that these low-molecular weight constructs have good tissue penetrating properties. Furthermore, we show that conjugation to a CPP endows the VHH-PS with an increased capacity to enter the cell via clathrin-mediated endocytosis at the expense of a slightly reduced affinity. These changed properties decreased PDT efficacy, suggesting that association with the cell membrane is needed for optimal therapeutic activity.

Acknowledgements

We thank Paul van Bergen en Henegouwen for the plasmid encoding 7D12. This work was supported by a grant from the Radboudumc.

Conflict of interest

No of the authors have a conflict of interest to declare.

Appendix A. Supplementary material

Supplementary data associated with this article can be found, in the online version, at https://doi.org/10.1016/j.ejpb.2017.12.009.

References

[1] B.W. Henderson, T.J. Dougherty, How does photodynamic therapy work? Photochem. Photobiol. 55 (1992) 145–157.
[2] J. Moan, K. Berg, The photodegradation of porphyrins in cells can be used to estimate the lifetime of singlet oxygen, Photochem. Photobiol. 53 (1991) 549–553.
[3] C. Holohan, S. Van Schaeybroeck, D.B. Longley, P.G. Johnston, Cancer drug resistance: an evolving paradigm, Nat. Rev. Cancer 13 (2013) 714–726.
[4] H. Kono, K.L. Rock, How dying cells alert the immune system to danger, nature reviews, Immunology 8 (2008) 279–289.
[5] D. van Straten, V. Mashayekhi, H.S. de Bruijn, S. Oliveira, D.J. Robinson, Oncologic photodynamic therapy: basic principles, current clinical status and future directions, Cancers (Basel) 9 (2017).
[6] J. Tian, L. Ding, H. Ju, Y. Yang, X. Li, Z. Shen, Z. Zhu, J.S. Yu, C.J. Yang, A multifunctional nanomicelle for real-time targeted imaging and precise near-infrared cancer therapy, Angew. Chem. Int. Ed. Engl. 53 (2014) 9544–9549.
[7] H. Ding, B.D. Sumer, C.W. Kessinger, Y. Dong, G. Huang, D.A. Boothman, J. Gao, Nanoscopic micelle delivery improves the photophysical properties and efficacy of photodynamic therapy of protoporphyrin IX, J. Control. Release: Off. J. Control. Release Soc. 151 (2011) 271–277.
[8] C.J. Rijcken, J.W. Hofman, F. van Zeeland, W.E. Hennink, C.F. van Nostrum, Photosensitiser-loaded biodegradable polymeric micelles: preparation, characterisation and in vitro PDT efficacy, J. Control. Release: Off. J. Control. Release Soc. 124 (2007) 144–153.
[9] S. Battah, S. Balaratnam, A. Casas, S. O'Neill, C. Edwards, A. Batlle, P. Dobbin, A.J. MacRobert, Macromolecular delivery of 5-aminolaevulinic acid for photodynamic therapy using dendrimer conjugates, Mol. Cancer Ther. 6 (2007) 876–885.
[10] A.M. Master, M.E. Rodriguez, M.E. Kenney, N.L. Oleinick, A.S. Gupta, Delivery of the photosensitizer Pc 4 in PEG-PCL micelles for in vitro PDT studies, J. Pharm. Sci. 99 (2010) 2386–2398.
[11] B. Li, E.H. Moriyama, F. Li, M.T. Jarvi, C. Allen, B.C. Wilson, Diblock copolymer micelles deliver hydrophobic protoporphyrin IX for photodynamic therapy, Photochem. Photobiol. 83 (2007) 1505–1512.
[12] A. Khdair, B. Gerard, H. Handa, G. Mao, M.P. Shekhar, J. Panyam, Surfactant-polymer nanoparticles enhance the effectiveness of anticancer photodynamic therapy, Mol. Pharm. 5 (2008) 795–807.
[13] V. Guillemard, H.U. Saragovi, Taxane-antibody conjugates afford potent cytotoxicity, enhanced solubility, and tumor target selectivity, Cancer Res. 61 (2001) 694–699.
[14] R. Heukers, P.M. van Bergen en Henegouwen, S. Oliveira, Nanobody-photosensitizer conjugates for targeted photodynamic therapy, Nanomedicine 10 (2014) 1441–1451.
[15] N. Mehraban, H.S. Freeman, Developments in PDT sensitizers for increased selectivity and singlet oxygen production, Materials (Basel) 8 (2015) 4421–4456.
[16] P.B. van Driel, M.C. Boonstra, M.D. Slooter, R. Heukers, M.A. Stammes, T.J. Snoeks, H.S. de Bruijn, P.J. van Diest, A.L. Vahrmeijer, P.M. van Bergen En, C.J. van de Henegouwen, C.W. Velde, D.J. Lowik, S Oliveira Robinson, EGFR targeted nanobody-photosensitizer conjugates for photodynamic therapy in a pre-clinical model of head and neck cancer, J. Control. Release 229 (2016) 93–105.
[17] S. Oliveira, G.A. van Dongen, M. Stigter-van Walsum, R.C. Roovers, J.C. Stam, W. Mali, P.J. van Diest, P.M. van Bergen en Henegouwen, Rapid visualization of human tumor xenografts through optical imaging with a near-infrared fluorescent anti-epidermal growth factor receptor nanobody, Mol. Imag. 11 (2012) 33–46.
[18] D. Kessel, J.J. Reiners Jr., Apoptosis and autophagy after mitochondrial or endoplasmic reticulum photodamage, Photochem. Photobiol. 83 (2007) 1024–1028.
[19] Y.J. Hsieh, C.C. Wu, C.J. Chang, J.S. Yu, Subcellular localization of Photofrin determines the death phenotype of human epidermoid carcinoma A431 cells triggered by photodynamic therapy: when plasma membranes are the main targets, J. Cell. Physiol. 194 (2003) 363–375.
[20] C. Pavani, A.F. Uchoa, C.S. Oliveira, Y. Iamamoto, M.S. Baptista, Effect of zinc insertion and hydrophobicity on the membrane interactions and PDT activity of porphyrin photosensitizers, Photochem. Photobiol. Sci.: Off. J. Eur. Photochem. Assoc. Eur. Soc. Photobiol. 8 (2009) 233–240.
[21] H. Li, T.Y. Tsui, W. Ma, Intracellular delivery of molecular cargo using cell-penetrating peptides and the combination strategies, Int. J. Mol. Sci. 16 (2015) 19518–19536.
[22] F. Milletti, Cell-penetrating peptides: classes, origin, and current landscape, Drug Discov. Today 17 (2012) 850–860.
[23] F. Duchardt, I.R. Ruttekolk, W.P. Verdurmen, H. Lortat-Jacob, J. Burck, H. Hufnagel, R. Fischer, M. van den Heuvel, D.W. Lowik, G.W. Vuister, A. Ulrich, M. de Waard, R. Brock, A cell-penetrating peptide derived from human lactoferrin with conformation-dependent uptake efficiency, J. Biol. Chem. 284 (2009) 36099–36108.

[24] S.A.M. van Lith, D. van den Brand, R. Wallbrecher, S.M.J. van Duijnhoven, R. Brock, W.P.J. Leenders, A conjugate of an Anti-Epidermal Growth Factor Receptor (EGFR) VHH and a cell-penetrating peptide drives receptor internalization and blocks EGFR activation, Chembiochem 18 (24) (2017) 2390–2394, http://dx.doi.org/10.1002/cbic.201700444.
[25] R.C. Roovers, T. Laeremans, L. Huang, S. De Taeye, A.J. Verkleij, H. Revets, H.J. de Haard, P.M. van Bergen en Henegouwen, Efficient inhibition of EGFR signaling and of tumour growth by antagonistic anti-EFGR Nanobodies, Cancer Immunol. Immunother. 56 (2007) 303–317.
[26] R.C. Roovers, M.J. Vosjan, T. Laeremans, R. el Khoulati, R.C. de Bruin, K.M. Ferguson, A.J. Verkleij, G.A. van Dongen, P.M. van Bergen en Henegouwen, A biparatopic anti-EGFR nanobody efficiently inhibits solid tumour growth, Int. J. Cancer 129 (2011) 2013–2024.
[27] G.T. Merlino, Y.H. Xu, S. Ishii, A.J. Clark, K. Semba, K. Toyoshima, T. Yamamoto, I. Pastan, Amplification and enhanced expression of the epidermal growth factor receptor gene in A431 human carcinoma cells, Science 224 (1984) 417–419.
[28] A.C. Navis, A. Bourgonje, P. Wesseling, A. Wright, W. Hendriks, K. Verrijp, J.A. van der Laak, A. Heerschap, W.P. Leenders, Effects of dual targeting of tumor cells and stroma in human glioblastoma xenografts with a tyrosine kinase inhibitor against c-MET and VEGFR2, PLoS One 8 (2013) e58262.
[29] M.N. Bijman, M.P. van Berkel, M. Kok, M.L. Janmaat, E. Boven, Inhibition of functional HER family members increases the sensitivity to docetaxel in human ovarian cancer cell lines, Anti-cancer Drugs 20 (2009) 450–460.
[30] Y. Kobashigawa, H. Kumeta, K. Ogura, F. Inagaki, Attachment of an NMR-invisible solubility enhancement tag using a sortase-mediated protein ligation method, J. Biomol. NMR 43 (2009) 145–150.
[31] R. Wallbrecher, W.P. Verdurmen, S. Schmidt, P.H. Bovee-Geurts, F. Broecker, A. Reinhardt, T.H. van Kuppevelt, P.H. Seeberger, R. Brock, The stoichiometry of peptide-heparan sulfate binding as a determinant of uptake efficiency of cell-penetrating peptides, Cell. Mol. Life Sci. 71 (2014) 2717–2729.
[32] M.E. Favretto, R. Brock, Stereoselective uptake of cell-penetrating peptides is conserved in antisense oligonucleotide polyplexes, Small 11 (2015) 1414–1417.
[33] J.D. Loike, S.C. Silverstein, A fluorescence quenching technique using trypan blue to differentiate between attached and ingested glutaraldehyde-fixed red blood cells in phagocytosing murine macrophages, J. Immunol. Methods 57 (1983) 373–379.
[34] E. de Boer, J.M. Warram, E. Hartmans, P.J. Bremer, B. Bijl, L.M. Crane, W.B. Nagengast, E.L. Rosenthal, G.M. van Dam, A standardized light-emitting diode device for photoimmunotherapy, J. Nucl. Med.: Off. Publ. Soc. Nucl. Med. 55 (2014) 1893–1898.
[35] V. Vichai, K. Kirtikara, Sulforhodamine B colorimetric assay for cytotoxicity screening, Nat. Protoc. 1 (2006) 1112–1116.
[36] M.F. Debets, S.S. van Berkel, S. Schoffelen, F.P. Rutjes, J.C. van Hest, F.L. van Delft, Aza-dibenzocyclooctynes for fast and efficient enzyme PEGylation via copper-free (3+2) cycloaddition, Chem. Commun. (Camb) 46 (2010) 97–99.
[37] S.A. van Lith, S.M. van Duijnhoven, A.C. Navis, W.P. Leenders, E. Dolk, J.W. Wennink, C.F. van Nostrum, J.C. van Hest, Legomedicine-A versatile chemo-enzymatic approach for the preparation of targeted dual-labeled llama antibody-nanoparticle conjugates, Bioconjug. Chem. 28 (2017) 539–548.
[38] I.D. Alves, C. Bechara, A. Walrant, Y. Zaltsman, C.Y. Jiao, S. Sagan, Relationships between membrane binding, affinity and cell internalization efficacy of a cell-penetrating peptide: penetratin as a case study, PloS One 6 (2011) e24096.
[39] D. Sarko, B. Beijer, R. Garcia Boy, E.M. Nothelfer, K. Leotta, M. Eisenhut, A. Altmann, U. Haberkorn, W. Mier, The pharmacokinetics of cell-penetrating peptides, Mol. Pharm. 7 (2010) 2224–2231.
[40] I.H. Madshus, E. Stang, Internalization and intracellular sorting of the EGF receptor: a model for understanding the mechanisms of receptor trafficking, J. Cell Sci. 122 (2009) 3433–3439.
[41] M. Carcenac, M. Dorvillius, V. Garambois, F. Glaussel, C. Larroque, R. Langlois, N.E. Hynes, J.E. van Lier, A. Pelegrin, Internalisation enhances photo-induced cytotoxicity of monoclonal antibody-phthalocyanine conjugates, Br. J. Cancer 85 (2001) 1787–1793.
[42] M. Mitsunaga, M. Ogawa, N. Kosaka, L.T. Rosenblum, P.L. Choyke, H. Kobayashi, Cancer cell-selective in vivo near infrared photoimmunotherapy targeting specific membrane molecules, Nat. Med. 17 (2011) 1685–1691.
[43] W. Zhong, J.P. Celli, I. Rizvi, Z. Mai, B.Q. Spring, S.H. Yun, T. Hasan, In vivo high-resolution fluorescence microendoscopy for ovarian cancer detection and treatment monitoring, Br. J. Cancer 101 (2009) 2015–2022.
[44] G.M. van Dam, G. Themelis, L.M. Crane, N.J. Harlaar, R.G. Pleijhuis, W. Kelder, A. Sarantopoulos, J.S. de Jong, H.J. Arts, A.G. van der Zee, J. Bart, P.S. Low, V. Ntziachristos, Intraoperative tumor-specific fluorescence imaging in ovarian cancer by folate receptor-alpha targeting: first in-human results, Nat. Med. 17 (2011) 1315–1319.